Analysis of collective spin-wave modes at different points within the hysteresis loop of a one-dimensional magnonic crystal comprising alternative-width nanostripes

S. Tacchi,[1] M. Madami,[1] G. Gubbiotti,[1,2] G. Carlotti,[1,3] S. Goolaup,[4] A. O. Adeyeye,[4] N. Singh,[5] and M. P. Kostylev[6]

[1]*CNISM, Unità di Perugia - Dipartimento di Fisica, Via A. Pascoli, I-06123 Perugia, Italy*

[2]*Istituto Officina dei Materiali del CNR (CNR-IOM), Unità di Perugia, c/o Dipartimento di Fisica, Via A. Pascoli, I-06123 Perugia, Italy*

[3]*CNR-Istituto di Nanoscienze, Centro S3, Via Campi 213A, I-41125 Modena, Italy*

[4]*Information Storage Materials Laboratory, Department of Electrical and Computer Engineering, National University of Singapore, 4 Engineering Drive 3, Singapore 117576, Singapore*

[5]*Institute of Microelectronics, 11 Science Park Road, Singapore Science Park II, Singapore 117685, Singapore*

[6]*School of Physics M013, University of Western Australia, 35 Stirling Hwy, 6009 Western Australia, Australia*

(Received 17 June 2010; revised manuscript received 7 October 2010; published 5 November 2010)

The Brillouin light-scattering technique has been applied to study collective spin waves in a dense array of dipolarly coupled $Ni_{80}Fe_{20}$ stripes of alternating widths, during the magnetization reversal process. Both the saturated "ferromagnetic" state, where the magnetizations of wide and narrow stripes are parallel, and the "antiferromagnetic" state, characterized by an antiparallel alignment of the static magnetization in adjacent stripes, have been analyzed. The experimental data provide strong evidence of sustained collective excitations in the form of Bloch waves with permitted and forbidden magnonic energy bands. The measured frequencies as a function of the exchanged wave vector have been satisfactorily reproduced by numerical simulations which enabled us to calculate the spatial profiles of the Bloch waves, showing that some of the modes are preferentially localized in either the wide or the narrow stripes. We estimated the expected light-scattering cross section for each mode at different magnetic ground states, achieving a good agreement with the measured intensities. The alternating-width stripes system studied here represents a one-dimensional artificial magnonic crystal with a complex base and can be considered as a model system for reprogrammable dynamical response, where the band structure of collective spin waves can be tailored by changing the applied magnetic field.

DOI: 10.1103/PhysRevB.82.184408 PACS number(s): 78.35.+c, 75.30.Ds, 75.75.Jn

I. INTRODUCTION

Brillouin light scattering (BLS) has proven to be a very powerful technique for direct measuring of the dispersion characteristics of magnons on periodic structures.[1] Ordered arrays of magnetic stripes with micrometric width served as model systems to shed light on the properties of spin-wave excitations in laterally confined magnetic elements. In numerous previous studies, magnetic excitations spectra have been measured in the case of noninteracting magnetic nanoelements, i.e., with negligible dipole-dipole interaction, revealing spin-wave modes standing along in-plane element sizes.[2,3]

Later, experimental and theoretical investigations were performed on arrays of either closely spaced stripes separated by air gaps[4–7] or alternated stripes of two different magnetic materials in direct contact.[8–10] All these systems are examples of one-dimensional (1D) magnonic crystals (MCs) where dipole-dipole interaction between stripes leads to the appearance of collective spin-wave modes propagating through the artificial crystal with oscillating and periodic frequency dispersion. Bands of allowed magnonic states are alternated with forbidden zones or band gaps. Therefore MCs are analogous to photonic crystals in optics[11] but spin waves at microwave frequencies, rather than light, are exploited to carry information.[12] Since the wavelength of spin excitations are much shorter than those of light in the gigahertz range, MCs offer better prospects for miniaturization at these frequencies with the advantage that frequency position and width of the band gap are tunable by the applied magnetic field.

A peculiar property of magnetic systems is the possibility of switching between several magnetic ground states by simply changing either the magnitude or the direction of the applied magnetic field. For instance, the magnetic order may not coincide with the geometrical one, giving rise to reprogrammable (reconfigurable) magnetic ground state.[13–15] However, in all previous BLS studies of collective spin modes in stripes arrays,[4–9] only the saturated state with equilibrium magnetization pointing along the stripes length has been considered. Thus the magnetic order for the investigated system coincided with the geometrical one.

In this work, we exploit BLS to investigate the evolution of *collective* spin-wave excitations on a 1D magnonic crystal, characterized by a complex unit cell, during the magnetization reversal process, encompassing both ferromagnetic (F) and antiferromagnetic (AF) magnetic ground states. The spin-wave frequencies have been measured as a function of the exchanged wave vector for a number of external field values within the hysteresis cycle. Numerical simulations are then performed to reproduce both the band structure and the cross section of the collective modes.

II. EXPERIMENTAL DETAILS

The sample investigated in this study consists of a periodic array of $L=40$ nm thick $Ni_{80}Fe_{20}$ nanostripes fabricated on a silicon substrate using deep ultraviolet lithography.[16]

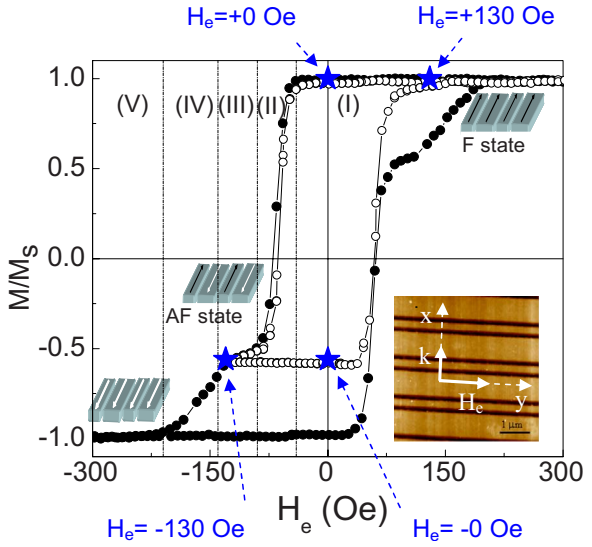

FIG. 1. (Color online) MOKE hysteresis loop for the sample (full dots). The open dots refer to the minor loop along which we performed BLS measurements, in correspondence of the four positions indicated by the stars. The lower inset shows the atomic force microscopy image of the stripes array, together with the reference system (the z axis is pointing out of plane), the direction of the applied field H_e and the direction of the spin-wave wave vector k in BLS measurements.

Each period consists of two stripes with different widths, w_n=330 nm and w_w=900 nm, alternating in the array, as shown in the atomic force microscopy image presented in the inset of Fig. 1. The edge-to-edge spacing between stripes is Δ=70 nm and the structure period is $a=w_n+w_w+2\Delta$ =1370 nm, corresponding to a Brillouin zone boundary of $\pi/a=2.3\times10^4$ rad/cm. The total length of the stripes is 4 mm so that negligible demagnetizing field is expected when they are longitudinally magnetized.

BLS spectra of the magnetic excitations were recorded by using a Sandercock (3+3)-pass tandem Fabry-Perot interferometer in the backscattering configuration. 200 mW of laser light (wavelength λ=532 nm) from a solid-state laser were focused through a camera objective (f-number 2 and 50 mm focal distance) onto the sample surface. This leads to an illuminated area of about 30×30 μm^2. A reversible magnetic field $\mathbf{H}_e$ was applied in the sample plane along the stripes length (y direction) and perpendicular to the incidence plane of light (Voigt geometry). Measurements were performed for different values of the incidence angle of light (θ), corresponding to different values of the transferred wave vector $k=(4\pi/\lambda)\sin(\theta)$ along the x direction (as shown in the inset of Fig. 1).

III. EXPERIMENTAL RESULTS AND QUALITATIVE DISCUSSION

A. Magnetization curve

The magnetization reversal mechanism for the sample under investigation has been extensively studied in Ref. 16. Here we briefly recall the main features of the magnetization curve (Fig. 1) measured by magneto-optic Kerr effect in the longitudinal configuration with the external field $\mathbf{H}_e$ applied along the stripes length (y direction). This corresponds to the stripes easy magnetization direction. The M-H loop is characterized by a double step process due to the distinct magnetization reversal of the nanostripes with different width.[17,18] As the field is reduced from positive saturation (Region I, F state) and reversed, a drop in magnetization, associated with the magnetization reversal of the family of wider nanostripes, occurs between about −40 and −90 Oe (Region II). This magnetization drop is proportional to the volume fraction of stripes which reverse their magnetization direction (w_w/w_n+w_w, i.e., 75% for our stripes array) and is in good agreement with the experimental result. Then a plateau is observed until the external field reaches about −140 Oe (Region III, AF state) where a second jump is seen which can be attributed to the reversal of magnetization in the narrower stripes (Region IV). This second jump is less sharp because intermediate states can be stabilized by dipolar interaction as far as clusters of stripes are switching and also because of the unavoidable presence of structural imperfections. Eventually, a reversed saturated state is attained for $H_e<-220$ Oe (Region V).

Note that in Fig. 1 we also show a measured minor hysteresis loop where it is seen that, coming from positive saturation, it is possible to attain the AF state for $H_e=-130$ Oe and this ground state remains stable if one comes back to zero field. This procedure has been exploited to prepare the system in the AF ground state at remanence.

B. BLS incidence-angle-resolved measurements

To study the characteristics of collective modes of the whole array their frequency was measured as a function of the exchanged wave vector k, along the direction perpendicular to the stripes (x direction). Figure 2 shows representative sequences of BLS spectra as a function of the incidence angle, for four different values of the external field, namely, H_e=+130 Oe, +0 Oe (this means zero field reached from +130 Oe), −130 Oe, and −0 Oe (this means zero field reached from −130 Oe). Note that, as inferred from the hysteresis loop shape, for the two former field values the magnetizations of both wide and narrow stripes are parallel (F state) while for the two latter values of the applied field the two families of stripes are antiparallel to each other (AF state), as sketched in the auxiliary diagrams of Figs. 1–3. For all the field values one sees that there are peaks which first increase their frequency and then decrease, and there are peaks with the opposite frequency variation. The oscillation amplitude (frequency width of the magnonic band) is more pronounced for the lowest frequency mode and decreases for the highest modes. This is in agreement with the prediction based on the modes' dipole (stray) fields outside stripes[19] and suggests that what we observe in Fig. 3 is the dispersion of collective Bloch waves, already seen in other studies.[6–9] Indeed, the periodicity in the k space for the dispersive modes matches the width of the first Brillouin zone ($2\pi/a=4.6\times10^4$ rad/cm) for this 1D magnonic crystal (note that here

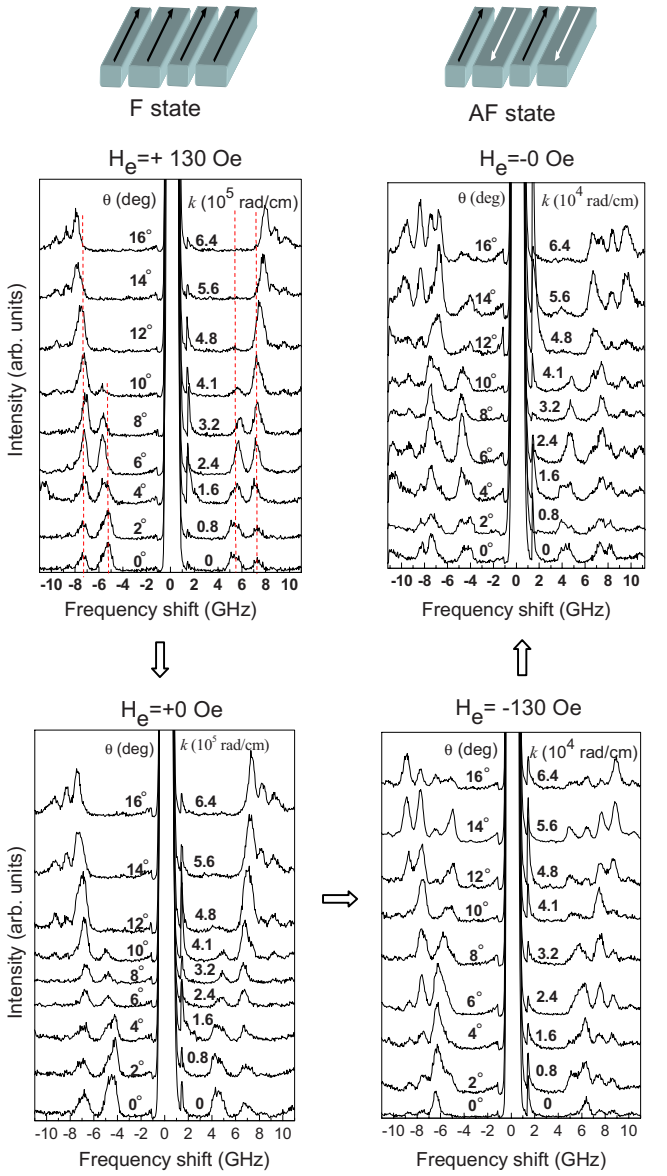

FIG. 2. (Color online) Experimental BLS spectra for k values and different applied fields. In the spectra of the left panels (H_e=+130 and +0 Oe) the stripes are coaligned while in those of right panels (H_e=−130 and −0 Oe) the magnetization in neighboring stripes is antiparallel. The notations +0 Oe and −0 Oe indicate that the zero field is reached from +130 Oe and −130 Oe, respectively.

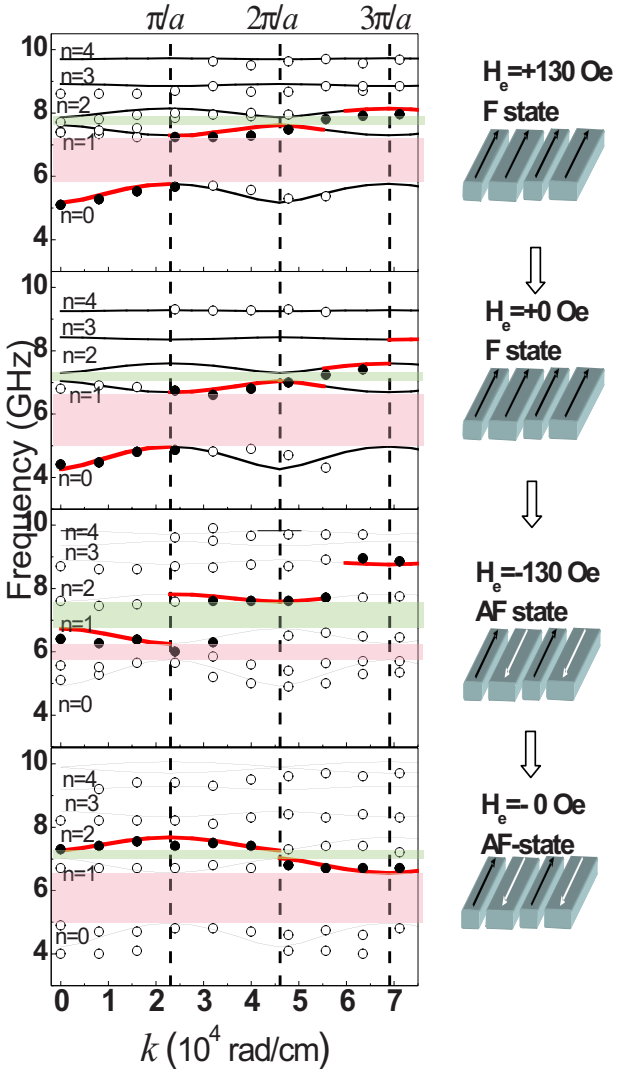

FIG. 3. (Color online) Sequence of measured (points) and calculated (lines) dispersion curves for different applied fields. (a): H_e=+130 Oe; (b): H_e=+0 Oe; (c) H_e=−130 Oe, and (d) H_e=−0 Oe. Full dots (bold lines) indicate the peak with the largest intensity in experimental (calculated) spectra. The shadowed areas correspond to the first two forbidden band gaps.

the periodicity in both the real and the reciprocal space does not change passing from F to AF state, different from what was observed in the case of arrays of stripes with identical width[15]). It is noteworthy that the intensity of the peaks changes with the angle of incidence, as seen in Fig. 2. Moreover, there is quite a strong difference in the peak intensity for the two sets of spectra recorded at +0 or −0 Oe, which only differ in the relative orientation of the two families of stripes. For example, the peak at 6.7 GHz which is observed at θ=16° for H_e=−0 Oe is completely absent in the corresponding spectrum at H_e=+0 Oe. This represents a clear evidence of the collective nature of the detected modes since it is clear that if the stripes were noninteracting, the spectra recorded in absence of the external field have to be the same for either parallel or antiparallel orientation of the magnetization in adjacent stripes.

IV. QUANTITATIVE INTERPRETATION OF THE DATA

A. Theoretical approach

To achieve a quantitative interpretation of the frequency and the intensity of collective excitations in the stripes array, we use the theory developed in Ref. 7, which assumes a long periodic magnetic order on the array. Based on Floquet (Bloch) theorem, dynamic magnetization for a collective Bloch wave can be written as

$$\tilde{\mathbf{m}}_{k_B}(x,z)\exp(ik_Bx). \tag{1a}$$

Here k_B is the Bloch wave number for the mode, x is the mode propagation direction in the array plane, and z is the

out-of-plane coordinate. The periodic Bloch function

$$\tilde{\mathbf{m}}_{k_B}(x,z) = \tilde{\mathbf{m}}_{k_B}(x+a,z), \tag{1b}$$

where a is the arrays periodicity, describes the mode profile in the reduced zone scheme.[4,19,20]

The equations in Refs. 4 and 19 allow treatment of present cases of both coalignment (FM state) and antialignment (AF state) of static magnetization in neighboring stripes. Indeed, the dynamic magnetization for the array obeys the Landau-Lifschitz magnetic torque equation, which for our system can be cast in the form

$$-i\omega\mathbf{m}(x,z) = -\gamma\{[\mathbf{M}(x)+\mathbf{m}(x,z)]\times[\mathbf{H}+\mathbf{h}(x,z)]\}, \tag{2}$$

where ω is the precession frequency. γ is the gyromagnetic coefficient, and $\mathbf{M}$ is the equilibrium magnetization, with $|M|$ equal to the film saturation magnetization M_s. The equilibrium magnetization depends on the position along the array periodicity x. It may be either coaligned with the axis y which is along the stripes or antialigned to it. The same applies to the internal static magnetic field $\mathbf{H}$ which is also applied in the array plane along the stripes. For instance, for the positive saturation for all stripes the projection of the static magnetization on the axis y,

$$M_y(x) = M_s \tag{3a}$$

and the static-field projection is $H_y=H_e$. For the experimental situation $H_e=-130$ Oe, one has

$$H_y = -130 \text{ Oe}$$

and

$$\begin{cases} M_y(x \text{ inside wider stripes}) = -M_s \\ M_y(x \text{ inside narrower stripes}) = M_s. \end{cases} \tag{3b}$$

In both cases in the gaps between stripes $M_y(x)=0$ (this is how the gaps are defined in this model).

As $\mathbf{M}$ and $\mathbf{H}$ are along y, the small linear dynamic magnetization component $\mathbf{m}$ has two components: one in the array plane (m_x) and one perpendicular to the array plane (m_z). This spatially inhomogeneous precessing magnetization gives rise to an effective field $\mathbf{h}$ which in our case of free oscillations consists of an effective exchange field

$$\mathbf{h}_{exc} = \alpha\nabla^2\mathbf{m}, \tag{4}$$

where α the exchange constant and of a dynamic dipole field $\mathbf{h}_d$ which is described by the magnetostatic equations. Solution of the magnetostatic equations is expressed in terms of a Green's function of dipole field,

$$\mathbf{h}_{dk}(x,z) = \int_S \hat{G}(x-x',z-z')\mathbf{m}(x',z')dx'dz'. \tag{5}$$

The integral is taken over the area S of cross section of the array in the x-z plane. Expressions for the components of the Green's function in the form which is the most suitable for numerical calculations can be obtained from the result in Ref. 21,

$$\begin{aligned} G_{zz}(\xi,\zeta) &= -G_{xx}(\xi,\zeta) - \delta(\xi)\delta(\zeta) \\ &= \lim_{\Delta z\to 0}\left\{\frac{1}{4\pi\Delta z}\ln\frac{(\xi^2+\zeta^2)^2}{[\xi^2+(\zeta-\Delta z)^2]^2[\xi^2+(\zeta+\Delta z)^2]^2}\right\}, \end{aligned} \tag{6a}$$

$$\begin{aligned} G_{zx}(\xi,\zeta) = G_{xz}(\xi,\zeta) &= -\lim_{\Delta z\to 0} \\ &\times\left[\frac{1}{4\pi\Delta z}\left(\operatorname{atan}\frac{\zeta+\Delta z}{\xi} - 2\operatorname{atan}\frac{\zeta}{\xi} + \operatorname{atan}\frac{\zeta-\Delta z}{\xi}\right)\right], \end{aligned} \tag{6b}$$

where $\xi=x-x'$ and $\zeta=z-z'$.

The physical meaning of the expressions above is the stray field of a magnetic stripe located at the position (x',z'). The stripe is infinitely long along y, infinitely thin along x, and has a thickness Δz along z. The field is averaged over the width Δz of the cross section of a similar infinitely thin and infinitely long stripe located at (x,z) [stripe edges have coordinates $(x,z-\Delta z/2)$ and $(x,z+\Delta z/2)$]. This Green's function is derived from the Green's function of the dipole field produced by a pointlike magnetic dipole $G_{\alpha,\beta}(\mathbf{r},\mathbf{r}') = -\frac{1}{4\pi}\frac{\partial}{\partial\alpha}\frac{\partial}{\partial\beta'}\frac{1}{|\mathbf{r}-\mathbf{r}'|}$, where α,β are x,y,z. The derivation is straightforward and consists in integration of the original Green's function over y', z', and z in the respective limits.

The formulation [Eq. (6)] is very convenient as in numerical calculations instead of taking the limit $\Delta z\to 0$ one chooses Δz equal to the discretization step along the array normal (axis z) and takes the values of the functions in the square brackets as approximations to the Green's-function components. Note that the expressions [Eq. (6)] are singular at $(\xi=0,\zeta=0)$. However the singularity is of a weak logarithmic type and can be eliminated by taking an improper double integral from $-\Delta x'/2$ to $\Delta x'/2$ and from $-\Delta x/2$ to $\Delta x/2$. The easiest way to take this integral is evaluating it numerically, by using standard methods of evaluation of improper integrals. This integration results in a field of an infinitely long rod of a rectangular cross section $\Delta x\times\Delta y$ at a distance $\sqrt{\xi^2+\varsigma^2}$ from its axis. The field is averaged over a rectangular cross section with the same area. In this formulation calculation of the total dipole field of dynamic magnetization is reduced to summation of fields produced by such rods.

Equations (2)–(6) form a homogeneous system of integrodifferential equations,

$$i\omega\mathbf{m} = \omega_H F(x)\begin{vmatrix} 0 & 1 \\ -1 & 0 \end{vmatrix}\mathbf{m} + \omega_M F(x)\alpha\hat{L}\mathbf{m} + \omega_M \times F(x)\hat{G}(x-x',z-z')\otimes F(x')\mathbf{m}(x',z') = 0. \tag{7}$$

Here $\tilde{\mathbf{m}} = \left|\begin{smallmatrix} m_x \\ m_z \end{smallmatrix}\right|$, $F(x)=M_y(x)/M_s$, $\omega_H(x)=\gamma H_y(x)$, $\omega_M = \gamma M_s$, $\hat{L}=\partial^2/\partial z^2+\partial^2/\partial x^2$ is a differential operator which follows from Eq. (4), $\hat{G}$ is the Green's function [Eqs. (5) and (6)], and $\otimes$ denotes the convolution operation.

One sees that the collective-mode eigenfrequency ω plays the role of the eigenvalue of the operator on the right-hand

side of Eq. (7). The vector eigenfunctions of the operator are then respective eigenprofiles of dynamic magnetization. The solution for Eq. (7) is given by Eq. (1). On substitution of this solution into Eq. (7) one obtains an equation for $\tilde{\mathbf{m}}_{k_B}(x,z)$. The new eigenfunctions are $\tilde{\mathbf{m}}_{k_B}(x,z)$, $\hat{L}$ takes the form $\partial^2/\partial z^2+\partial^2/\partial x^2-k_B^2$ and instead of $\hat{G}$ one has

$$\sum_{n=-\infty}^{\infty} \hat{G}(x-x'-na)\exp[-ik_B(x-x'-na)]\exp(-|n|a/l_c). \tag{8}$$

While deriving Eq. (8) we took advantage of translational symmetry of the solution along x [Eq. (1b)]. This approach corresponds to the standard formulation of dispersion in periodic media in the reduced zone scheme,[4,19,20] where the area of definition for the integrodifferential operator reduces just to one structure period which makes it suitable for numerical treatment.

While deriving Eq. (8) we also phenomenologically introduced the coherence length l_c for collective modes.[7,19] (It is convenient to express the coherence length in a number of lattice constants.) This parameter is completely phenomenological and is justified in the following way. In our experience the theory usually overestimates the frequency width of the magnonic zones or real manonic crystals (see Fig. 6 in Ref. 5). The equations above do not contain any fitting parameter to adjust the width of the magnonic zones while keeping all the other characteristics of the collective-mode dispersion the same. On the other hand, numerically the decrease in the zone width can be obtained by truncating the series in Eq. (8) before the series properly converges. Therefore one may suppose that the discrepancy is an artifact of numerical calculation and arises from the well-known property of bad convergence of the dipole sums. However, it is not the case of Eq. (8): truncation of this particular sum at $n=\pm 10$ and $n=\pm 50$ gives results which overlap with graphical accuracy.

Therefore we believe that experimentally measured dispersion is always smaller than calculated because of imperfectness of the real magnonic crystals. Some deviation from perfect periodicity, such as slightly varying stripe widths, slight variation in the stripe positions on the lattice, and rounded up stripe edges may reduce dipole coupling of very distant neighbors. The introduced parameter l_c accounts for this reduced dipole coupling by effectively truncating the series in Eq. (8) earlier.

As in our previous works, in this work the eigenvalue-eigenfunction problem is solved numerically. Representing the structure period in the form of the two-dimensional (2D) stack of the rods transforms the operator [Eqs. (7)] into a matrix. The eigenvector/eigenvalue problem for the matrix is solved using the complex QR algorithm.[22] This is made for a number of Bloch wave numbers k_B across the first two Brillouin zones for the magnonic crystal.

We divide the structure period into 64 rods along x ($\Delta x=21$ nm) and 9 rods along the thickness z ($\Delta z=4.4$ nm). This ensures error in frequency below 200 MHz, which is better than the experimental accuracy. (Increasing Δx by 2 times reduces the frequency for the fundamental mode by 300 MHz.) A decrease in Δx by two times changes the frequency by just 10 MHz. Importantly, in both cases the dispersion curve is moved up or down *as a whole* but its slope which determines the width of the fundamental magnonic band does not vary with graphical accuracy.

B. Comparison between measured and calculated dispersion curves

The curves reported in Fig. 3 are the result of our calculation of the dispersion curves (ω vs k) for the collective excitations on the stripes array. We first performed a best fit of the experimental data for $H_e=+130$ Oe to the curves calculated assuming that magnetization in all stripes on the array is aligned with the applied magnetic field and that the stripes are magnetically saturated. From this procedure, we extracted the following material parameters for the collective excitations:[7] saturation magnetization $4\pi M_s=7800$ G, gyromagnetic coefficient $\gamma=2\pi\times 2.8$ rad/μs, and collective-mode coherence length equal to 4.5 structure periods.[19] These values of parameters were also used in the numerical calculations for the other field values [Figs. 3(b)–3(d)] achieving a good agreement with the experimental data at any field value.

In order to analyze in more details the dispersion curves of Fig. 3, it is very useful to illustrate the spatial profiles of the different modes. These are obtained as the eigenfunctions of the same integrodifferential operation used to calculate the modes eigenfrequencies (see above).

C. Illustration of the calculated mode profiles

In Fig. 4 we show the mean value for both components of vector $\tilde{\mathbf{m}}_{k_B}(x,z)$ over z as a function of x, for the four different values of the external field H_e used in the experiment: +130, +0, −130, and −0 Oe (the meaning of +0 and −0 Oe is the same as in the previous section). The discrete modes are labeled according to the integer index $n=0,1,2,\ldots$

First a general comment on the mode profiles. Physically the collective modes represent coupled standing-wave resonances of the so-called Damon-Eshbach (DE) type waves in a continuous magnetic film.[23] This wave has a surface character and the waves propagating in different directions are localized at the opposite film surfaces (the out-of-plane wave number k_z is imaginary). In the confined geometry of the stripe this effect of surface localization results in the fact that the wave is not completely standing. There is some circulation of amplitude around the perimeter of the stripe cross section. This is clearly seen from 2D profiles of the phase of the complex amplitude of dynamic magnetization. The closer to the stripe upper ($z=40$ nm) or lower ($z=0$) surfaces the larger is the portion of the travelling wave in the total energy. However, overall this portion is small and most of the resonance energy is contained in the standing wave.[24] Let us now proceed to the main discussion. We start with a comment on the behavior of the lowest frequency mode ($n=0$). First one notices that when the stripes are in the F state ($H_e=+130$ and +0 Oe) the sign of both the in-plane and the out-of-plane components of the dynamical magnetization are the same in

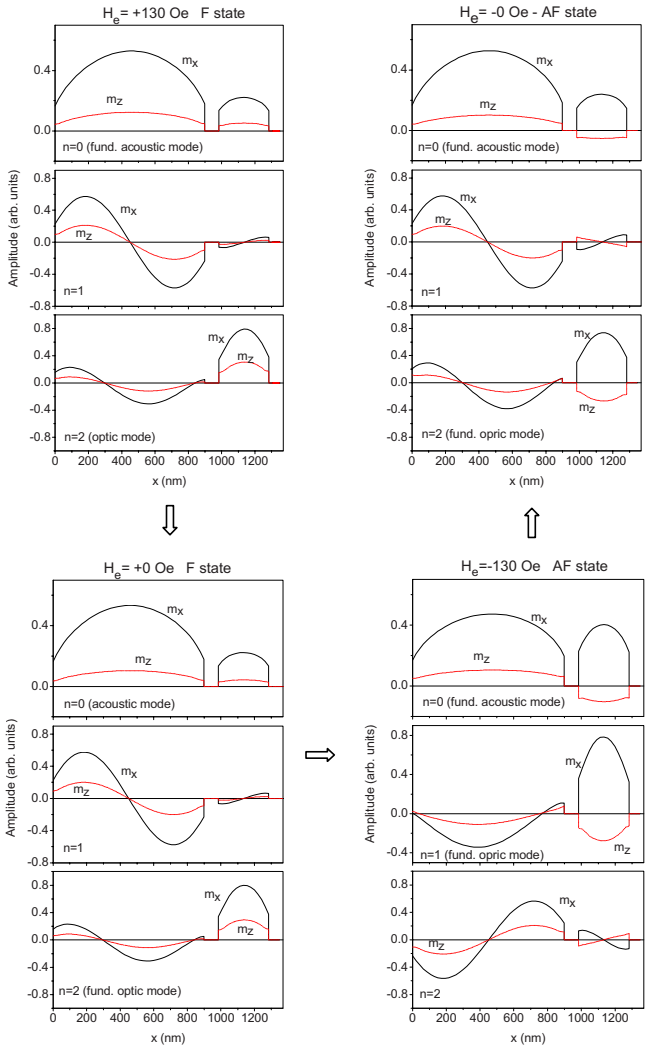

FIG. 4. (Color online) Calculated mode profiles for the three lowest modes ($n=0$, $n=1$, and $n=2$) at the same field values of the previous two figures. Solid lines: in-plane component of the dynamic magnetization $\tilde{m}_{k=0,x}$; dashed lines: out-of-plane component $\tilde{m}_{k=0,z}$. The values averaged over the structure thickness L, i.e., along z, are shown.

both wide and narrow stripes. This means that the magnetization precession is in phase in the two families of stripes. However, at $H_e=-130$ and -0 Oe, when one has to deal with the AF state, the sign of the out-of-plane component in narrow and wide stripes is opposite. This is due to the fact that in this case the sense of precession of magnetization in narrow stripes is opposite to those in wide stripes. (This situation is similar to the exchange coupled bilayer films, see Fig. 2 in Ref. 25). For instance at $H_e=-130$ Oe, for the lowest frequency mode ($n=0$) the in-plane components $\tilde{m}_{k_B{}^x}$ of $\tilde{\mathbf{m}}_{k_B}$ for the wider and the narrower stripes are in phase but the out-of-plane components $\tilde{m}_{k_B{}^z}$ are in the antiphase. For the first higher order mode ($n=1$) the situation is opposite: the out-of-plane components $\tilde{m}_{k_B{}^z}$ are in phase and the in-plane components $\tilde{m}_{k_B{}^x}$ are in antiphase. Now, since $\tilde{m}_{k_B{}^x} \gg \tilde{m}_{k_B{}^z}$ (due to a strong ellipticity of precession magnetization in Permalloy) one may consider the lowest mode ($n=0$) as an analogue of the fundamental acoustic mode for the doublet, and the first higher order one ($n=1$) as its fundamental optic mode, whose amplitude of precession is considerably larger in the narrower stripes than in the wider ones. (Note however that at $H_e=+130$, $+0$, and -0 Oe the fundamental optic mode coincides with the $n=2$ mode.)

This may be explained by the fact that, given the considerable width difference between the stripes, the lowest resonant eigenfrequency for *uncoupled* narrow stripes is higher than for uncoupled wide ones. Therefore, when the stripes are interacting one may expect that the lower frequency (acoustic) mode of the doublet formed from the fundamental modes for uncoupled stripes of both types (fundamental doublet) will be characterized by a larger amplitude of precession in the wider stripes, and the upper frequency (optic) mode by a larger amplitude (i.e., by larger localization of the amplitude of oscillation) in the narrower stripes. We checked this idea by making calculations for different values of the interstripe distance Δ. It was found that with increase in Δ the dipole coupling decreases and the acoustic (optic) mode for the doublet gradually transforms into the fundamental mode for uncoupled wide (narrow) stripes, which confirms this idea.

Considerable amplitude localization in narrow stripes is clearly seen in Fig. 4 for the fundamental optic mode (recall that it corresponds to $n=1$ at $H_e=-130$ and $n=2$ at the other field values). Instead, for the fundamental acoustic mode ($n=0$) the amplitude localization in wide stripes is less pronounced since it is clear that the impact of the larger stripes onto magnetic dynamics in the narrower ones is much more pronounced than the impact of the narrower ones onto the wider ones.

Remarkably, the considerable localization of the amplitude of the optic mode in narrower stripes explains the important difference in frequencies for this mode for $H_e=+130$ and -130 Oe. In the former case this mode is positioned between 7 and 8 GHz, and in the latter case it is situated between 6 and 7 GHz. The reason for this downshift can be found in the fact that for $H_e=+130$ Oe the magnetization of narrow stripes is coaligned with the applied field while for $H_e=-130$ Oe it is antiparallel to the applied magnetic field so that the frequency for the optic collective mode drops significantly. As a consequence of the above downshift of the $n=1$ mode, it is seen in Fig. 3 that the amplitude of the main forbidden band gap is significantly reduced at $H_e=-130$ Oe.

Finally, it is worth noticing that the frequency of this mode (as well as for all the other modes) for $H_e=+0$ and -0 Oe is practically the same. This evidences that the contribution of the out-of-plane component of dynamic magnetization to the collective dipole field of the array is negligible due to large ellipticity of precession. Thus the in-plane component of dynamic magnetization, only, is responsible for formation of the collective dynamics.

As a final remark about the measured mode frequencies, for the case of AF magnetic ground state ($H_e=-130$ and -0 Oe), there are some extra points in Fig. 3 at low frequency, below the $n=0$ mode. We attribute their presence and the increased scattering of the experimental data to the magnetic disorder on the array during the reversal process. A

detailed study of the effect of disorder during reversal will be the object of a separate forthcoming work.

D. Comparison between measured and calculated BLS cross section

One interesting experimental evidence which can be observed in the sequences of spectra of Fig. 2 is that the relative intensity of the detected peaks is strongly dependent on both the ground state of the magnetization and the exchanged wave-vector value. In Fig. 3 we reported as full points the frequency of the most intense peak in each spectrum. We then took advantage from the calculated mode profiles illustrated in the previous section to estimate the expected intensity of the BLS peaks thanks to the simple model of BLS response proposed by Stashkevich *et al.* in the Appendix of Ref. 26. According to this model, one has to consider two effects which are relevant for determining the intensity of each BLS peak: the conservation of the wave vector and the magneto-optical interaction. (We do not include the contribution from the density of magnon states which is related to the steepness of the dispersion slope[27] into this simple calculation.)

The conservation of the wave vector implies that the BLS intensity of each eigenmode collected at some transferred wave number k is proportional to the squared modulus of the Fourier component with the same value of Fourier wave number of the complete eigenprofile of dynamic magnetization (Fourier-component consideration). It follows that allowing k_B to take values outside the first Brillouin zone permits an easy calculation of both the mode dispersion and the amplitude of the respective Fourier component of the dynamic magnetization.[27] In fact, the Fourier component for a transferred wave vector $k=k_B$ equals to the mean value of $\tilde{\mathbf{m}}_{k_B}(x,z)$ along x over one structure period. For simplicity we neglect the decay of the light intensity across the element thickness (along z). Then the BLS response for a mode is proportional to the mean value of the vector $\tilde{\mathbf{m}}_{k_B}(x,z)$ both across the sample width and the structure period. The Fourier-component contribution of the $n=0$ acoustic mode is the largest in the first BZ while the $n=1$ mode dominates in the second BZ, etc. This tendency of a prevailing nth mode in the nth-1 BZ is clearly observed in the experiment when one studies the F state ($H_e=+130$ and $+0$ Oe), as seen in the upper panels of Fig. 3. However, a similar analysis of the data for the AF state ($H_e=-130$ and -0 Oe) reveals a different behavior. Before explaining this difference let us consider the magneto-optical grounds of BLS process (magneto-optical consideration). In fact, at normal incidence ($k=0$) the in-plane component of dynamic magnetization does not contribute to the BLS cross section at all [see Eq. (2) in Ref. 28]. This means that the BLS intensity depends on the out-of-plane component of dynamic magnetization $\tilde{m}_{k_Bz}$, solely. As one can see from Fig. 4, the ellipticity of precession $\varepsilon_p = |\tilde{m}_{k_Bx}/\tilde{m}_{k_Bz}|$ is about 5 and 3 for $n=0$ and $n=2$, respectively. Therefore one may expect a dramatic change in intensity with the incidence angle, when magnetization vector precesses in different senses in stripes of different type. It is a straightforward procedure to calculate the relative intensities

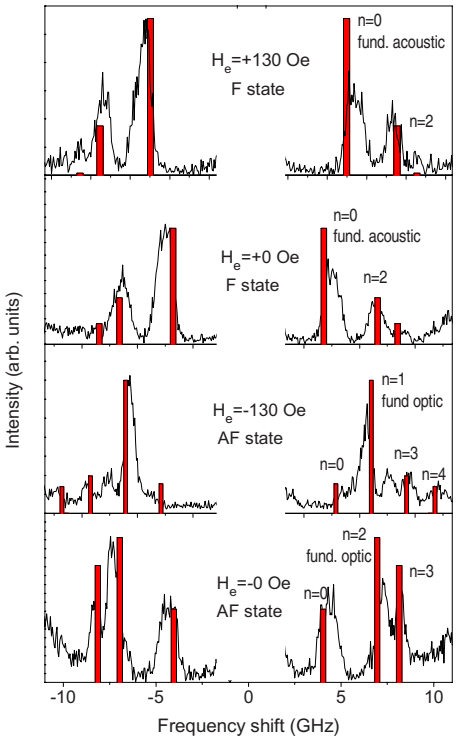

FIG. 5. (Color online) Comparison between experimental BLS spectra at $k=0$ and calculated BLS intensity for the four field values used in previous figures. The calculated intensity of each peak is represented by a red bar (placed in the position of the calculated mode frequency) whose height corresponds to the calculated cross section for the corresponding mode.

using the expressions in Ref. 26. The only parameter needed is the complex permittivity of the material at optical frequencies. We assume that for Permalloy ($Ni_{80}Fe_{20}$) it is the same as for Nickel: $\varepsilon=-5+12i$ (refractive index: $n=2+3i$).

The results of our calculations are shown by the bold lines in Fig. 3. Each bold curve indicates the mode with the most intense BLS response for a particular transferred wave number k. Moreover, in Fig. 5 we compare the calculated intensities for the first four modes with the experimental spectra for the most relevant and simple case of normal incidence ($k=0$).

As stated above, one sees that the theory correctly predicts that for $k=0$ and the F ground state ($H_e=+130$ and $+0$ Oe in Figs. 3 and 5) the largest BLS response is for the $n=0$ fundamental acoustic mode while for the AF state the intensity of the same mode for $k=0$ is considerably smaller than those of higher order modes. In fact, from Fig. 4 one sees that the z component of the net dynamic magnetic moment is considerably smaller for the fundamental acoustic mode than for the fundamental optical mode, resulting in a lower intensity for the former mode ($n=0$) with respect to the latter ($n=1$ for $H_e=-130$ Oe and $n=2$ for $H_e=-0$ Oe). However, as follows from the theory in Ref. 26, with increase in the incidence angle the contribution from the large in-plane component $\tilde{m}_{k_Bx}$ should increase and the fundamental mode should become visible. This is confirmed by our calculations and is clearly seen in our experimental data (Figs. 2 and 3).

In the centre of the second BZ ($k=2\pi/a$), where magnetization profiles are the same as for $k_B=0$, both the "Fourier-component" and the "magneto-optic" considerations lead to a dominating cross section for the mode with the antisymmetric profile, which also has different numbers n for different H_e values: $n=1$ for $H_e=+130$, -0, and $+0$ Oe but $n=2$ for $H_e=-130$ Oe (see Fig. 4).

Two important deductions can be drawn from the above consideration. (i) The small intensity for the fundamental acoustic mode ($n=0$) for the AF state for the normal incidence is the clear *signature* of the strong dynamical dipole coupling between stripes since only phase locking of dynamic magnetization in the narrower stripes to the one in the wider stripes may produce the small intensity seen for this mode in the AF state. (ii) The difference in intensities for the fundamental and the first higher order mode can be used to *probe* the ground state of an array of dynamically dipole coupled elements. The best illustration for this conclusion comes from direct comparison of the data for $H_e=+0$ and -0 Oe in Fig. 5.

V. CONCLUSION

We have experimentally studied collective spin-wave excitations of a dense periodic array of dipolarly coupled magnetic stripes of alternating width. This is a prototype of a one-dimensional magnonic crystal, where the ground state and the consequent dynamic response are field controlled. In the saturated F state the Brillouin light scattering response in Voigt geometry had the form of a number of discrete peaks. Periodical variation in peaks frequencies as a function of the exchanged wave vector k suggested strong dipole coupling of the stripes and formation of travelling collective excitations on the arrays. As usually, the largest BLS intensity for small k values was observed for the fundamental mode of the collective excitations

Upon reversing the applied magnetic field, an AF state, characterized by an antiparallel alignment of the static magnetization in the adjacent stripes, was formed due to the different coercivity of the $Ni_{80}Fe_{20}$ stripes having different width. In contrast to the F state, in the AF state and in the small-angle incidence conditions the response for the higher order fundamental optic mode dominated in the BLS intensity spectra. Our numerical simulations showed that the decreased amplitude for the fundamental acoustic mode is a clear signature of the strong dynamic dipole coupling on the array inside the hysteresis loops. This shows that collective spin-wave excitations can be used as a probing tool of magnetic order periodicity inside the hysteresis cycle. Furthermore, it was found that the forbidden band gaps can substantially modified by changing the magnetic ground state and the intensity of the applied field.

ACKNOWLEDGMENTS

The authors acknowledge the European Community's Seventh Framework Programme (FP7/2007-2013) under Grant Agreement No. 228673 (MAGNONICS). Support by Australian Research Council, the University of Western Australia, Ministero Italiano dell'Università e della Ricerca (MIUR) under the PRIN2007 project (Project No. 2007X3Y2Y2), and Ministry of Education, Singapore under Project No. R263-000-437-112 is also acknowledged. We also thank A. A. Stashkevich for fruitful discussions.

[1] S. O. Demokritov and B. Hillebrands, in *Spin Dynamics in Confined Magnetic Structures I*, Topics in Applied Physics Vol. 83, edited by B. Hillebrands and K. Ounadjela (Springer-Verlag, Berlin, 2002), p. 65, and references therein.

[2] B. Hillebrands, in *Novel Techniques for Characterizing Magnetic Materials*, edited by Y. Zhu (Springer, New York, 2005).

[3] Y. Roussigné, S. M. Chérif, and P. Moch, J. Phys.: Condens. Matter **16**, 4591 (2004).

[4] M. P. Kostylev, A. A. Stashkevich, and N. A. Sergeeva, Phys. Rev. B **69**, 064408 (2004).

[5] G. Gubbiotti, S. Tacchi, G. Carlotti, P. Vavassori, N. Singh, S. Goolaup, A. O. Adeyeye, A. Stashkevich, and M. Kostylev, Phys. Rev. B **72**, 224413 (2005).

[6] G. Gubbiotti, S. Tacchi, G. Carlotti, N. Singh, S. Goolaup, A. O. Adeyeye, and M. Kostylev, Appl. Phys. Lett. **90**, 092503 (2007).

[7] M. Kostylev, P. Schrader, R. L. Stamps, G. Gubbiotti, G. Carlotti, A. O. Adeyeye, S. Goolaup, and N. Singh, Appl. Phys. Lett. **92**, 132504 (2008).

[8] Z. K. Wang, V. L. Zhang, H. S. Lim, S. C. Ng, M. H. Kuok, S. Jain, and A. O. Adeyeye, Appl. Phys. Lett. **94**, 083112 (2009).

[9] Z. K. Wang, V. L. Zhang, H. S. Lim, S. C. Ng, M. H. Kuok, S. Jain, and A. O. Adeyeye, ACS Nano **4**, 643 (2010).

[10] N. I. Polushkin, Phys. Rev. B **77**, 180401(R) (2008).

[11] K. Sakoda, *Optical Properties of Photonic Crystals* (Springer-Verlag, Berlin, 2001).

[12] V. V. Kruglyak, S. O. Demokritov, and D. Grundler, J. Phys. D: Appl. Phys. **43**, 264001 (2010).

[13] F. Giesen, J. Podbielski, T. Korn, M. Steiner, A. van Staa, and D. Grundler, Appl. Phys. Lett. **86**, 112510 (2005).

[14] S. Neusser and D. Grundler, Adv. Mater. **21**, 2927 (2009).

[15] J. Topp, D. Heitmann, M. P. Kostylev, and D. Grundler, Phys. Rev. Lett. **104**, 207205 (2010).

[16] S. Goolaup, A. O. Adeyeye, N. Singh, and G. Gubbiotti, Phys. Rev. B **75**, 144430 (2007).

[17] M. H. Kryder, K. Y. Ahn, N. J. Mazzeo, S. Schwarzi, and S. M. Kane, IEEE Trans. Magn. **16**, 99 (1980).

[18] J. I. Martín, J. Nogués, Kai Liu, J. L. Vicent, and Ivan K. Schuller, J. Magn. Magn. Mater. **256**, 449 (2003).

[19] G. Gubbiotti, S. Tacchi, M. Madami, G. Carlotti, A. O. Adeyeye, and M. Kostylev, J. Phys. D: Appl. Phys. **43**, 264003 (2010).

[20] C. Bayer, M. P. Kostylev, and B. Hillebrands, Appl. Phys. Lett. **88**, 112504 (2006).

[21] G. Gubbiotti, M. Kostylev, N. Sergeeva, M. Conti, G. Carlotti, T. Ono, A. N. Slavin, and A. Stashkevich, Phys. Rev. B **70**, 224422 (2004).

[22] J. H. Wilkinson and C. Rinsch, *Handbook for Automatic Com-*

putation: Linear Algebra (Springer-Verlag, Berlin, 1971), Vol. 2.

[23] R. W. Damon and J. R. Eshbach, J. Phys. Chem. Solids **19**, 308 (1961).

[24] The reason for this is as follows. The out-of-plane wave number for DE waves equals to the in-plane wave number ($|k_z|=|k_x|$) (Ref. 23). The in-plane *standing-wave* wave number for the fundamental resonance mode for the narrow stripes corresponds the value $\pi/w_n \cong 10^5$ rad/cm and for the wide ones by $\pi/w_w \cong 3.5\times 10^4$ rad/cm. Given the stripe thickness $L=40$ nm, one obtains $\exp(-|k_z|L)=0.7$ and 0.87 for the narrow and the wide stripes, respectively. Therefore at the stripe surfaces the travelling wave contribution to the total resonance energy is about $[\exp(|k_z|0)-0.87]^2=2\%$ for the wide stripes and about 10% for the narrow ones and it decreases toward the stripe middle. For this reason presenting in Fig. 4 the profiles averaged over the film thickness is appropriate for the discussion below.

[25] R. L. Stamps, Phys. Rev. B **49**, 339 (1994).

[26] A. A. Stashkevich, Y. Roussigné, P. Djemia, S. M. Chérif, P. R. Evans, A. P. Murphy, W. R. Hendren, R. Atkinson, R. J. Pollard, A. V. Zayats, G. Chaboussant, and F. Ott, Phys. Rev. B **80**, 144406 (2009).

[27] M. P. Kostylev and A. A. Stashkevich, Phys. Rev. B **81**, 054418 (2010).

[28] R. Zivieri, P. Vavassori, L. Giovannini, F. Nizzoli, E. E. Fullerton, M. Grimsditch, and V. Metlushko, Phys. Rev. B **65**, 165406 (2002).